Elastic In-Plane Stiffness for a Circular Cut Reduced Beam Section (RBS)

NESTOR R. IWANKIW and JAMSHID MOHAMMADI

A great amount of steel research has been conducted nationally after the 1994 Northridge earthquake to identify modified steel moment connections for improved structural resistance and ductility to higher seismic demands. FEMA 350 (FEMA, 2000) and the AISC *Seismic Provisions for Structural Steel Buildings* (AISC, 2002) summarize most of these significant advancements and new technical information for seismic design of structural steel buildings.

One popular newer moment connection that has been introduced and validated (prequalified) during these last few years for use in high seismic areas is the so-called "dogbone," or reduced beam section (RBS). Earlier papers (Iwankiw and Carter, 1996; Iwankiw, 1997; Engelhardt, Winneberger, Zekany, and Potyraj, 1996; Engelhardt, Winneberger, Zekany, and Potyraj, 1998; Engelhardt, 1999; Zekioglu, Mozaffarian, Le Chang, and Uang, 1997; and others) contain the genesis, structural behavior, and design intent of this newer ductile detail, which in contrast to the extended family of reinforced steel moment connections (with haunches, flange cover plates, ribs), efficiently accomplishes the desired formation of an internal beam plastic hinge (ductile "fuse") through controlled removal of a small portion of the beam flanges near the member ends. The preferred RBS cut geometry is now circular (Engelhardt, 1999) as shown in Figure 1, and that is the only profile that will be explicitly considered in this paper, even though other cut profiles could be similarly analyzed.

In the development of the RBS, it was clearly recognized that there would be some accompanying stiffness loss with this detail relative to the usual prismatic (unreduced) beam section. Prior work (Iwankiw, 1997 and Engelhardt, 1999) has provided a few selected or approximate answers, together with a generalization that the expected beam stiffness loss is relatively modest for most cases, roughly on the order of a maximum 10 percent for the typical RBS conditions. FEMA 350 also contains recommendations for estimating this RBS stiffness reduction for new construction. AISC *Design Guide 12* (Gross, Engelhardt, Uang, Kasai, and Iwankiw, 1999), among many other matters, lists all the then up-to-date experimental results on RBS cyclic tests, and the possible adaptation of the RBS to the retrofit of existing steel buildings.

In contrast to simply using reduced stiffness estimates or ignoring them altogether as relatively insignificant, discretized RBS modeling, and more refined analysis, can be conducted on an individual, and as needed, project basis to determine the actual stiffnesses. Such an exact and complete stiffness solution may be desirable in some cases to enable more accurate lateral frame stiffness and drift computations and checking under service conditions. However, this may be somewhat difficult and time-consuming. Therefore, the purpose of this paper is to briefly review the basic in-plane stiffness formulation for a prismatic beam, develop more rigorously the full non-prismatic, first-order elastic stiffness changes caused by the circular RBS, provide its simplified representation, and finally conclude with the general RBS stiffness effect suggestions for design. Other RBS seismic design and performance issues of this efficient and popular detail will not be addressed here, as they are already well covered in the other available, and previously referenced, sources.

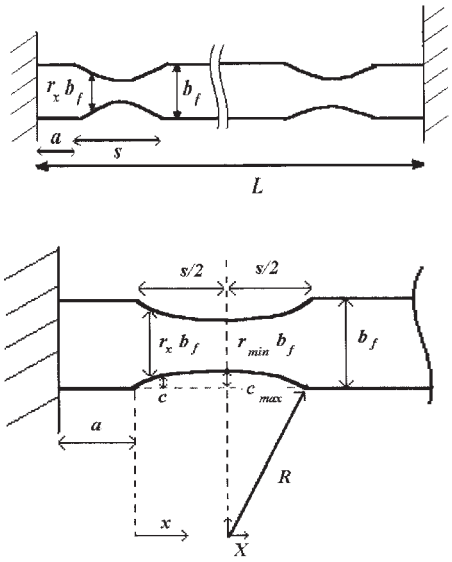

Fig. 1. Circular Cut Geometry.

Nestor R. Iwankiw is senior engineer & director, Hughes Associates, Inc., Chicago, IL.

Jamshid Mohammadi is professor, Illinois Institute of Technology, Chicago, IL.

REVIEW OF PRISMATIC BEAMS

The fundamental two-dimensional (planar) beam element, with three degrees of freedom at each end (two translations and one rotation) is illustrated in Figure 2. Accordingly, elastic small displacement theory is used without any coupling of flexure-axial effects. For this prismatic (constant area, A, and moment of inertia, I) beam section, elementary linear-elastic principles lead to the following well-established 6×6-member stiffness matrix in the local coordinate system, multiplied by E/L.

$$(E/L)\begin{bmatrix} 4I & 2I & \frac{6I}{L} & \frac{-6I}{L} & 0 & 0 \\ 2I & 4I & \frac{6I}{L} & \frac{-6I}{L} & 0 & 0 \\ \frac{6I}{L} & \frac{6I}{L} & \frac{12I}{L^2} & \frac{-12I}{L^2} & 0 & 0 \\ \frac{-6I}{L} & \frac{-6I}{L} & \frac{-12I}{L^2} & \frac{12I}{L^2} & 0 & 0 \\ 0 & 0 & 0 & 0 & A & -A \\ 0 & 0 & 0 & 0 & -A & A \end{bmatrix} \quad (1)$$

where

E = Young's modulus of elasticity
I = member moment of inertia about the strong bending axis
A = member cross-section area
L = member span length

The underlying basis for these common flexural stiffness values lies in the following expressions that are derivable from simple beam theory. Through appropriate substitutions and simplification, this entire member 6×6 matrix can be written as in Equation 2, only in terms of the individual member bending stiffness properties K_{11} and K_{12}, and the axial stiffness K_{55}, where K_{ij} is the force or moment in the "i" direction due to unit displacement or rotation in the "j" direction:

$$\begin{bmatrix} K_{11} & K_{12} & \frac{(K_{11}+K_{12})}{L} & -\frac{(K_{11}+K_{12})}{L} & 0 & 0 \\ K_{12} & K_{22} & \frac{(K_{11}+K_{12})}{L} & -\frac{(K_{11}+K_{12})}{L} & 0 & 0 \\ \frac{(K_{11}+K_{12})}{L} & \frac{(K_{11}+K_{12})}{L} & K_{33}=\frac{2(K_{11}+K_{12})}{L^2} & -K_{33} & 0 & 0 \\ -\frac{(K_{11}+K_{12})}{L} & -\frac{(K_{11}+K_{12})}{L} & -K_{33}=\frac{-2(K_{11}+K_{12})}{L^2} & K_{33} & 0 & 0 \\ 0 & 0 & 0 & 0 & K_{55} & -K_{55} \\ 0 & 0 & 0 & 0 & -K_{55} & K_{55} \end{bmatrix} \quad (2)$$

K_{11} = moment at end 1 due to a unit rotation at end 1, equals $4EI/L$ for prismatic case
K_{12} = moment at end 1 due to a unit rotation at end 2, equals $2EI/L$ for prismatic case
K_{33} = shear at end 1 due to unit transverse displacement at end 1, equals to $12EI/L^3$ for prismatic case
K_{55} = axial force at end 1 due to axial displacement at end 1, equals to AE/L for prismatic case

Notice the familiar conclusion that due to the Maxwell-Betti Reciprocal Theorem, this beam stiffness matrix is diagonally symmetric, in other words $K_{ij} = K_{ji}$. Also, like action stiffness terms are equal, in other words, $K_{11} = K_{22}$ for moment-rotation, $K_{33} = K_{44}$ for shear-translation, and $K_{55} = K_{55}$ for axial-displacement. The upper left 4×4 sub matrix represents the beam first order flexural properties, while the lower right 2×2 sub matrix gives the linear axial effect. With these convenient simplifications in the usual stiffness matrix formulation, it becomes evident that there are really only three independent stiffness parameters which can fully define all the individual terms of the planar elastic beam stiffness matrix: K_{11} and K_{12}, or K_{11} and $(K_{11} + K_{12})$, or K_{11} and

$$K_{33} = \frac{2(K_{11} + K_{12})}{L^2},$$

and other similar combinations for the 16 flexural terms, and K_{55} for the 4 axial terms.

Another reminder of this governing K_{11} and K_{12} effect for the flexural beam response is, the traditional slope-deflection equation:

$$M_1 = \frac{EI}{L}\left(K_{11}\theta_1 + K_{12}\theta_2 - (K_{11} + K_{12})\frac{\Delta}{L} \right) \quad (3)$$

where

θ_1, θ_2 = rotation at end 1 and end 2, respectively
Δ = transverse relative deflection between end 1 and 2

Also, the moment distribution procedure uses the so-called carry-over factor, wherein the relationship between the beam rotational stiffnesses K_{11} and K_{12} is given as:

$$K_{12} = qK_{11}$$

Fig. 2. Beam in-Plane Degrees of Freedom.

where

q = moment carry-over factor, equal to 0.5 for prismatic conditions

Therefore, since the prismatic beam element can be completely characterized for linear elastic response by only three independent stiffness parameters (say K_{11} for moment-rotation, K_{33} for transverse shear-displacements, and K_{55} for axial effects), a straightforward approach to completely determine the non-prismatic stiffnesses of an RBS can be developed. It would first require the derivation of these same three parameters for the RBS member with the circular cut, and then their computational extension to its full beam stiffness matrix.

RBS STIFFNESS FORMULATION

The main RBS assumptions for this development are that the flange reductions (size and location) are circular and completely symmetric in the beam, both relative to the top and bottom flanges as well as to the left and right halves of the beam span, and representative of typical/reasonable RBS geometries, in other words size ranges of rolled wide-flange beams and beam spans controlled by flexural behavior.

For such a symmetric RBS, the

$$K_{11}^{RBS}, K_{33}^{RBS}, \text{ and } K_{55}^{RBS}$$

stiffnesses will be determined, which will then lead to the full characterization of its modified elastic stiffness matrix for the non-prismatic case. In order to accomplish this in an easy and transparent manner, first define an RBS reduced stiffness factor, Q, associated with each of these three primary stiffnesses relative to their prismatic counterparts K_{11}, K_{33}, and K_{55}:

$$Q_{11} = \frac{K_{11}^{RBS}}{K_{11}} \le 1.0 \tag{5}$$

$$Q_{33} = \frac{K_{33}^{RBS}}{K_{33}} \le 1.0 \tag{6}$$

$$Q_{55} = \frac{K_{55}^{RBS}}{K_{55}} \le 1.0 \tag{7}$$

A prismatic member defaults to a Q value of 1.0 for all of its stiffness terms, while an RBS will have Q values less than 1.0. This means that the resulting effective RBS stiffness parameter, K_{ij}^{RBS}, can simply be expressed as $Q_{ij}K_{ij}$, where K_{ij} is the associated property for the prismatic case, and Q_{ij} is its accompanying reduction factor. Since there are only three independent stiffness parameters, say

$$K_{11}^{RBS}, K_{33}^{RBS}, \text{ and } K_{55}^{RBS},$$

similarly there will exist only the three correspondingly independent Q_{11}, Q_{33}, and Q_{55}. The dependent Q_{12} reduction may be computed from the relationships that

$$K_{33}^{RBS} = \frac{2\left(K_{11}^{RBS} + K_{12}^{RBS}\right)}{L^2} \tag{8}$$

and

$$K_{12}^{RBS} = Q_{12}K_{12} \tag{9}$$

which after these substitutions and use of $K_{11} = 4EI/L$, $K_{33} = 12EI/L^3$, $K_{55} = AE/L$, $K_{12} = K_{11}/2 = 2EI/L$ for the prismatic case, and subsequent simplifications results in

$$Q_{12} = 3Q_{33} - 2Q_{11} \tag{10}$$

Under this format, the full RBS stiffness matrix can be symbolically given in Equation 11 in terms of the three Q reduced stiffness factors multiplying the corresponding matrix terms of the prismatic member given previously in Equation 1.

The Q_{33} factor applies not only to the diagonal K_{33} and K_{44} shear terms, but also to all the other combination translational stiffness terms that include the sum of $(K_{11} + K_{12})$, in other words a majority of the flexural portion of the member stiffness matrix.

$Q_{11}K_{11}$	$Q_{12}K_{12}$	$Q_{33}\frac{(K_{11}+K_{12})}{L}$	$-Q_{33}\frac{(K_{11}+K_{12})}{L}$	0	0
$Q_{12}K_{12}$	$Q_{22}K_{22}$	$Q_{33}\frac{(K_{11}+K_{12})}{L}$	$-Q_{33}\frac{(K_{11}+K_{12})}{L}$	0	0
$Q_{33}\frac{(K_{11}+K_{12})}{L}$	$Q_{33}\frac{(K_{11}+K_{12})}{L}$	$Q_{33}K_{33}$	$-Q_{33}K_{33}$	0	0
$-Q_{33}\frac{(K_{11}+K_{12})}{L}$	$-Q_{33}\frac{(K_{11}+K_{12})}{L}$	$-Q_{33}K_{33}$	$Q_{33}K_{33}$	0	0
0	0	0	0	$Q_{55}K_{55}$	$-Q_{55}K_{55}$
0	0	0	0	$-Q_{55}K_{55}$	$Q_{55}K_{55}$

(11)

Also, if needed, the moment carry-over factor, q, can be determined from

$$q = \frac{K_{12}^{RBS}}{K_{11}^{RBS}} = \frac{Q_{12}K_{12}}{Q_{11}K_{11}} = \frac{Q_{12}}{2Q_{11}} \tag{12}$$

CIRCULAR CUT GEOMETRY

Figure 1 shows the representative circular cut profile that is assumed for the RBS, and its primary geometric variables: c_{max}, c, R, b_f, a, s, r_{min}, and r_x.

- c = flange width reduction on each side of beam centerline
- b_f = standard wide-flange width of original beam
- a = RBS offset distance from member end
- c_{max} = maximum beam flange reduction per side at RBS center
- s = total length of RBS
- r_x = varying flange width coefficient within the RBS
- r_{min} = minimum RBS flange width coefficient at the maximum flange reduction

Because of RBS symmetry, at the RBS centerline (maximum section reduction)

$$(1 - r_{min})\, b_f = 2c_{max} \tag{13}$$

and, in general within the RBS,

$$(1 - r_x)\, b_f = 2c \tag{14}$$

From this, it follows that

$$\frac{c_{\max}}{L} = \frac{(1 - r_{\min})}{2}\left(\frac{b_f}{L}\right) \tag{15}$$

The geometric equation of a circle can be written in the following form that shows its radius, R, as a function of the RBS c_{max} and s distances:

$$R = \frac{\left(4c_{\max}^2 + s^2\right)}{8c_{\max}} \tag{16}$$

From this central expression and the circular cut geometry relative to the RBS centerline coordinate "X" (see Figure 1), the variation in the flange width reduction, c, can be computed from:

$$c = \sqrt{R^2 - X^2} - \sqrt{R^2 - \left(\frac{s}{2}\right)^2} \tag{17}$$

It was decided to non-dimensionalize all these variables in anticipation of conducting a subsequent parametric study, primarily through division by the beam span, L, or the beam depth, d. From before, recall that

$$r_x = 1 - \frac{2c}{b_f} \tag{18}$$

After non-dimensionalization in this manner, and after a translation of the local abscissa coordinate for each RBS cut relative to the left starting edge (rather than its center) of $X = x - s/2$ results in

$$r_x = \frac{1 - 2\left(\sqrt{\left(\frac{R}{L}\right)^2 - \left(\frac{x}{L} - \frac{s}{2L}\right)^2} - \sqrt{\left(\frac{R}{L}\right)^2 - \left(\frac{s}{2L}\right)^2}\right)}{\left(\frac{b_f}{2}\right)} \tag{19}$$

with

$$\frac{R}{L} = \frac{4\left(\frac{c_{\max}}{L}\right)^2 + \left(\frac{s}{L}\right)^2}{\frac{c_{\max}}{L}} \tag{20}$$

$b_f/L = b_f/d/(L/d)$, since b_f/d is a section shape property, and L/d is the commonly used beam span-to-depth ratio.

Again due to symmetry, it can easily be shown that the RBS effect on the flange moment of inertia about its strong axis is a linear function of "r_x", in other words,

$$I_f^{RBS} = r_x I_f$$

where

- I_f^{RBS} = varying moment of inertia about its strong axis due to the RBS flanges only
- I_f = moment of inertia of original beam about its strong axis due to only the flanges

Then, since only the RBS flanges were reduced, the varying total moment of inertia within the RBS, I_x, is simply

$$I_x = I_f^{RBS} + I_w = r_x I_f + (I - I_f) = I - I_f(1 - r_x) \tag{21}$$

where

- I = total original beam moment of inertia about its strong axis
- I_w = moment of inertia of beam due to only the web

or, by nondimensionalizing,

$$\frac{I_x}{I} = 1 - \frac{I_f}{I}(1 - r_x) \tag{22}$$

The RBS circular cut geometry and varying inertial property are now sufficiently and conveniently defined in terms of several key nondimensional problem and shape input

parameters that will enable its subsequent stiffness solution. The conjugate beam method is used to subsequently determine the flexural RBS stiffness parameters

$$K_{11}^{RBS} \text{ and } K_{33}^{RBS}$$

or Q_{11} and Q_{33}, respectively, while the flexibility method is used to determine the axial stiffness $K_{55}^{RBS}$and its corresponding Q_{55} reduced stiffness factor. For convenience, in the subsequent RBS formulation, the "RBS" superscript for the various stiffness terms is dropped, in other words,

$$K_{11} = K_{11}^{RBS}, K_{33} = K_{33}^{RBS}, \text{ etc.}$$

BENDING STIFFNESS SOLUTION

In accordance with fundamental principles, the conjugate beam method offers a convenient solution for elastic rotations and transverse displacements through use of an equivalent beam loading by the original bending moment diagram divided by the member's *EI*. The resulting shears of this conjugate beam are the actual rotations of the original beam, and the bending moments are its displacements (elastic curve). This conjugate beam analogy effectively transforms the solution of the governing differential equations, or alternative energy-based or virtual work formulations, for elastic rotations and displacements into another beam mechanics problem that can be readily handled using ordinary moment and shear calculations well familiar to structural engineers. Most elementary textbooks on structural analysis and mechanics of materials present the essentials of the method's formulation and application. In summary, the key steps are:

1. Convert real beam into its conjugate beam with appropriate modification of its boundary conditions.

2. Determine bending moment diagram, *M*, of original beam.

3. Divide this moment diagram by the member flexural stiffness, *EI*, and apply this *M/EI* as new distributed loading over the conjugate beam span.

4. Compute the shears and moments of the conjugate beam, which are the desired elastic rotations and deflections, respectively, of the real beam.

For flexural stiffness parameter determination, the basic case is that of a fixed-fixed beam subjected to imposed unit end rotation or displacement. The equivalent conjugate beam for a fixed-fixed real boundary condition is simply a free-free member loaded by the applicable rotational end moments, divided by *EI*. This latter step accounts for the possible non-prismatic nature of the member, such as an RBS. The imposition of the unit end rotation boundary condition for the stiffness problem also, thereby, prescribes a known end shear of unity in the conjugate beam, (see Figure 3a), say at the left end, where the K_{11} moment will also then be applied, and K_{12} at the right beam end.

With this conjugate beam model for a prescribed unit end rotation, as illustrated in Figures 3a and 3b, the general solution is obtained for the primary RBS bending stiffness terms K_{11} and K_{12} by simply enforcing equilibrium for the conjugate beam forces and moments, in other words equilibrium of the K_{11}/EI and K_{12}/EI diagrams with the unit end reaction at the "11" member end. This nonprismatic RBS condition introduces the obvious varying EI_x complication in what would otherwise have been a routine calculation for the linear K_{11} and K_{12} moments for constant *EI* in a prismatic member. This key difference is reflected in the enlarged curved portions of the conjugate beam distributed loading within the RBS regions, since the RBS flexural stiffness EI_x within the RBS length, *s*, or in non-dimensional form *s/L*, varies with distance and is less than the original *EI*. Using the previously developed functional relationships for the circular cut RBS, EI_x, or EI_x/I in non-dimensional form from the previous section, is established in a local coordinate system for each RBS length in the left and right halves of the beam span, because the transverse

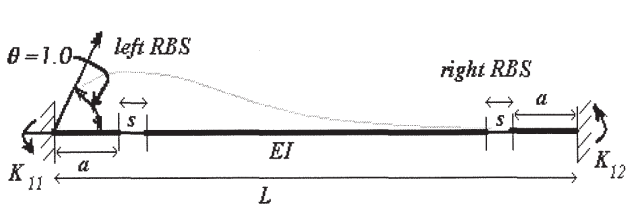

Fig. 3a. RBS Bending Stiffness Model.

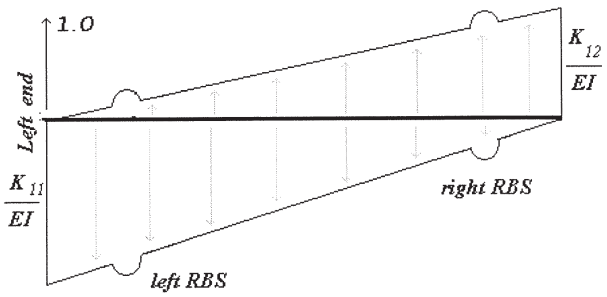

Fig. 3b. Equivalent Conjugate Beam Loading.

Table 1. W-Shape Section Property Range

Shape Series		b_f/d	I_f/I	A_f/A
All	minimum	0.297	0.689	0.430
	maximum	1.05	0.964	0.818
	average	0.538	0.845	0.640
Larger than W18	minimum	0.297	0.693	0.434
	maximum	0.606	0.894	0.705
	average	0.427	0.823	0.599

loading differs between the left and right sides due to the moment gradient. Further explanation and details of this solution procedure are given in Appendix A.

In summary, this type of an RBS stiffness solution for its flexural stiffness parameters, formulated on the basis of fundamental beam theory, and the conjugate beam analogy, is accurate, transparent and straightforward, even though it involves many individual computational steps.This entire procedure is very amenable to programming on spreadsheet software. Use of Simpson's rule within the RBS segments simplifies the otherwise mathematically difficult closed-form integrations, which, nevertheless, have been recently independently developed by other authors (Chambers, Stenger, and Almudhafar, 2003).

AXIAL STIFFNESS SOLUTION

The linear elastic axial stiffness change in the RBS is relatively easy to assess next. Because of the full symmetry of this new problem (both RBS are uniformly affected by axial extension or contraction, in other words, constant axial force, in contrast to the previous flexural analysis that required a separate left and right side RBS evaluation due to moment gradient), it is only necessary to consider a single RBS segment of length *s/L* within the beam half-span.

Application of the elementary axial flexibility equations over the prismatic and RBS segments, respectively, of the beam provides the following total axial deformation resulting from a uniform unit axial force:

$$\delta_{11} = \frac{L}{AE}\left(1-\frac{2s}{L}\right)+\frac{2L}{AE}\int_{o}^{\left(\frac{s}{L}\right)}\frac{\left(\frac{dx}{L}\right)}{1-\left(\frac{A_f}{A}\right)\left(1-r_x\right)} \tag{23}$$

Non-dimensional variables and properties were again used consistent with the previous flexural solution for the RBS flange width coefficient "r_x." Similar to the moment of inertia variation within the RBS, the section area variation can be represented as indicated above, with A_f/A substituted for the previous I_f/I,

where

A_f = area of the flanges of the original beam = $2b_ft_f$

Also, as for the flexural stiffness analysis, Simpson's rule was used with n =10 to perform a numerical integration over *s/L* of the RBS term, wherein the corresponding axial integrand function is

$$y = \frac{1}{1-\frac{A_f}{A}(1-r_x)} \tag{24}$$

Because, by definition, stiffness is the inverse of flexibility, the axial RBS reduced stiffness in terms of *AE/L* becomes

$$Q_{55} = 1/\delta_{11} \tag{25}$$

This axial part of the RBS stiffness computations can also be programmed, together with its flexural counterparts, into a spreadsheet for a computerized solution.

DESIGN LIMITS FOR WIDE FLANGE SECTIONS

This problem was intentionally formulated in terms of several non-dimensional parameters. As seen from the prior RBS formulations, the following basic input values for dimension and section property ratios are required for this complete stiffness analysis:

L/d = span to depth ratio
b_f/d = ratio of flange width to depth
r_{min} = defined previously

I_f/I = ratio of flange to total moment of inertia about strong axis
A_f/A = ratio of flange to total area
a/L = ratio of RBS offset distance from member end to span length
s/L = ratio of RBS length to span length

Because one of the additional purposes of this work was to conduct a parametric sensitivity study of typical wide-flange beams with a RBS, it became necessary to identify the practical range of b_f/d, I_f/I, and A_f/A property ratios that would be realistically encountered in standard rolled beams.The prequalification limits of the RBS as provided in FEMA 350 (FEMA, 2000) include wide-flange beams up to a maximum size of W36×300.

The current AISC shapes database was used to search and sort these section properties, and the results (minimum, maximum, and average) are presented in Table 1 for all wide flange shapes, and those with nominal depths greater than or equal to 18 in. (common beam sections). On this basis, the following general bounds were selected for the input RBS properties:

$$0.7 \le \frac{I_f}{I} \le 0.9$$

$$0.4 \le \frac{A_f}{A} \le 0.8$$

$$0.3 \le \frac{b_f}{d} \le 0.6$$

Based on other published RBS design criteria and common beam applications, see Iwankiw and Carter (1996), Iwankiw (1997), Engelhardt (1996), and Engelhardt (1999), it was also decided to constrain the other problem input as follows:

$$0.05 \le \frac{s}{L} \le 0.1$$

$$0.025 \le \frac{a}{L} \le 0.1$$

$$0.5 \le r_{\min} \le 0.65$$

$$5 \le \frac{L}{d} \le 20$$

Implicit in these bounds is the recognition that RBS applications were developed for flexurally controlled beam spans, that the RBS is adjacent to the member end and is of relatively short length, and that the RBS cuts typically remove 35 to 50 percent of the flange width, but no more than 50 percent.

With the definitions of all these specific independent input values, the remaining dependent parameters b_f/L, c_{max}/L, and R/L can be accordingly quantified, such that the only variables are the x/L integration distance within the RBS, and the unknowns to be determined: q, K_{11}, and Q_{55}. A readily available check on this entire procedure is to verify that all Q's indeed default to 1.0, and to q =0.5, for a prismatic case, in other words, s/L = 0.0 or r_{min} = 1.0.

PARAMETRIC STUDY AND STATISTICAL REGRESSION

The intended nature of this RBS stiffness formulation made it very convenient to conduct a parametric study, and subsequently a regression analysis, of the cases that covered the design range of practical interest. The common multivariate "least squares" method of the first order (linear) was employed for this regression analysis, with the intent that it could present a much quicker, but sufficiently accurate, means to determine the RBS stiffness effects. The particular ranges of interest for the input parameters were given in the preceding section. The final results of these 40 RBS case solutions and their regression estimates are given in Table 2 for the Q_{33} cases. The exact RBS solution for each case according to the methods summarized before is indicated by Q_{33}, and its regression estimate by Q_{33}^{est}, as given in Table 2. Similar results and comparisons were also made for Q_{11} to determine the following regression equation:

$$Q_{11}^{est} = 0.9357 - 0.7845\left(\frac{s}{L}\right) + 0.2983\left(\frac{a}{L}\right) + 0.2309\left(r_{\min}\right) - 0.1293\left(\frac{I_f}{I}\right) \quad (26)$$

It quickly became obvious during the course of these initial statistical sensitivity studies that both the L/d and b_f/d variables did not have a major effect on the RBS flexural stiffness estimates, hence they were eliminated from the final output. The conclusion is that both the span and section property dependency are already adequately captured by the four other non-dimensional parameters in the regression formulation. However, it is important to ensure that the RBS is used within the regression range of its design variables, including a flexurally controlled span-to-depth ratio and a flange cut range of 35 to 50 percent (r_{min} between 0.65 and 0.50). Notice that because of the latter, the regression estimates are not valid for cuts smaller than 35 percent of the beam flange width (or r_{min} greater than 0.65), including the prismatic case of r_{min} = 1.0. The estimated errors will be higher, and likely significantly so, when outside the stated range of the regression variables as analyzed. For these sit-

Table 2. Regression Results for Q_{33}

Q_{33}	s/L	a/L	r_{min}	I_f/I	Q_{est}	Q_{est}/Q
0.9520	0.050	0.025	0.65	0.70	0.9554	1.0036
0.9183	0.100	0.025	0.65	0.70	0.9131	0.9943
0.9662	0.050	0.100	0.65	0.70	0.9853	1.0198
0.9430	0.100	0.100	0.65	0.70	0.9429	0.9999
0.9238	0.050	0.025	0.50	0.70	0.9167	0.9923
0.8745	0.100	0.025	0.50	0.70	0.8743	0.9998
0.9458	0.050	0.100	0.50	0.70	0.9465	1.0008
0.9112	0.100	0.100	0.50	0.70	0.9041	0.9923
0.9227	0.050	0.100	0.50	0.90	0.9176	0.9945
0.8754	0.100	0.100	0.50	0.90	0.8752	0.9998
0.8924	0.050	0.025	0.50	0.90	0.8878	0.9948
0.8266	0.100	0.025	0.50	0.90	0.8454	1.0227
0.8883	0.050	0.025	0.50	0.90	0.8878	0.9994
0.8250	0.100	0.025	0.50	0.90	0.8454	1.0247
0.9196	0.050	0.100	0.50	0.90	0.9176	0.9978
0.8741	0.100	0.100	0.50	0.90	0.8752	1.0013
0.9346	0.050	0.025	0.65	0.90	0.9265	0.9914
0.8901	0.100	0.025	0.65	0.90	0.8842	0.9933
0.9536	0.050	0.100	0.65	0.90	0.9564	1.0029
0.9227	0.100	0.100	0.65	0.90	0.9140	0.9906
0.9527	0.050	0.100	0.65	0.90	0.9564	1.0039
0.9223	0.100	0.100	0.65	0.90	0.9140	0.9910
0.9333	0.050	0.025	0.65	0.90	0.9265	0.9927
0.8896	0.100	0.025	0.65	0.90	0.8842	0.9939
0.8924	0.050	0.025	0.50	0.90	0.8878	0.9948
0.8266	0.100	0.025	0.50	0.90	0.8454	1.0227
0.9227	0.050	0.100	0.50	0.90	0.9176	0.9945
0.8754	0.100	0.100	0.50	0.90	0.8752	0.9998
0.9210	0.050	0.025	0.50	0.70	0.9167	0.9953
0.8733	0.100	0.025	0.50	0.70	0.8743	1.0011
0.9438	0.050	0.100	0.50	0.70	0.9465	1.0029
0.9103	0.100	0.100	0.50	0.70	0.9041	0.9932
0.9511	0.050	0.025	0.65	0.70	0.9554	1.0046
0.9179	0.100	0.025	0.65	0.70	0.9131	0.9947
0.9655	0.050	0.100	0.65	0.70	0.9853	1.0205
0.9427	0.100	0.100	0.65	0.70	0.9429	1.0002
0.9249	0.050	0.025	0.50	0.70	0.9167	0.9911
0.8749	0.100	0.025	0.50	0.70	0.8743	0.9993
0.9466	0.050	0.100	0.50	0.70	0.9465	0.9999
0.9115	0.100	0.100	0.50	0.70	0.9041	0.9919

Q_{33} MIN = 0.8250; max ($Qest/Q$) ≈ 1.02; Std Error of Estimate 0.00876; No. of Observations = 40
Q_{33} MAX = 0.9662; min ($Qest/Q$) ≈ 0.99; R Squared = 0.94863; Degrees of Freedom = 35

$$Q_{33}^{est} = 0.9210 - 0.8476\left(\frac{s}{L}\right) + 0.3981\left(\frac{a}{L}\right) + 0.2585\left(r_{\min}\right) - 0.1446\left(\frac{I_f}{I}\right)$$

Table 3. Regression Results for Q_{55}

Q_{55}	s/L	A_f/A	r_{min}	Q_{est}	Q_{est}/Q
0.9890	0.05	0.400	0.65	0.9979	1.0090
0.9790	0.10	0.400	0.65	0.9979	0.9989
0.9830	0.05	0.400	0.50	0.9829	0.9999
0.9690	0.10	0.400	0.50	0.9629	0.9937
0.9590	0.05	0.800	0.50	0.9561	0.9970
0.9250	0.10	0.800	0.50	0.9361	1.0120
0.9760	0.05	0.800	0.65	0.9711	0.9950
0.9530	0.10	0.800	0.65	0.9511	0.9980
0.9830	0.05	0.600	0.65	0.9845	1.0015
0.9670	0.10	0.600	0.65	0.9645	0.9974
0.9720	0.05	0.600	0.50	0.9695	0.9974
0.9490	0.10	0.600	0.50	0.9495	1.0005

Q_{55} MIN = 0.925; max ($Qest/Q$) ≈ 1.01; Std Error of Estimate 0.00604; No. of Observations = 12
Q_{55} MAX = 0.989; max ($Qest/Q$) ≈ 0.99; R Squared = 0.91888; Degrees of Freedom = 8

$$Q_{55}^{est} = 0.9796 - 0.4\left(\frac{s}{L}\right) - 0.0669\left(\frac{A_f}{A}\right) + 0.100\, r_{min}$$

uations, for example, when $r_{min} > 0.65$, the exact solution should be used. The statistical correlation coefficient (R squared) for both Q_{11}^{est} and Q_{33}^{est} was very high, about 0.95, and the standard error of the estimate was less than 0.009, both indicating that the resulting predictor expressions account for most of the RBS flexural stiffness variability with relatively little error. This fact is further confirmed in Table 2 by observing the ratios of Q^{est}/Q, wherein the maximum range of this predictor-to-exact ratio is about +2 percent to −1 percent.

Proceeding similarly for the RBS axial stiffness Q_{55}, Table 3 presents the exact solutions and regression results based upon its primary variables s/L, A_f/A and r_{min}. In contrast to the flexural Q_{11} and Q_{33}, the axial Q_{55} is independent of the other bending related variables, as expected. Again, an excellent confidence measure (R squared) of about 0.92, and low standard error of the estimate of 0.006, was obtained for the Q_{55}^{est} (see Table 3), despite the fact that only 12 cases were analyzed for this much simpler axial effect. The maximum Q_{est}/Q ratio was also a correspondingly low ±1 percent.

Therefore, simple linear regression equations for

$$Q_{11}^{est},\ Q_{33}^{est},\ \text{and}\ Q_{55}^{est}$$

can provide a very reasonable, and accurate, design alternative to the exact stiffness solution within the given bounds of the respective RBS design variables. The sensitivity of the resulting estimate to the design parameters is explicitly given in the form of the various regression coefficients for the variables.

EXAMPLE

A recent paper (Chambers and others, 2003) contains an independent derivation of the RBS elastic stiffness changes based on a closed-form virtual work solution. The example in this publication describes the following problem with its given input:

Beam W24×76:

I = 2100 in.^{4} (strong axis)
d = 23.92 in.
L = 216 in.
A = 22.4 in.^{2}
I_f = 1651 in.^{4}
I_f/I = 0.79, ok
L/d = 9.03 > 5, and < 20, ok
b_f = 8.99 in.
t_f = 0.68 in.
b_f/d = 0.376, ok
A_f = 12.23 in.^{2}
A_f/A = 0.546, ok

RBS:

s = 20 in.
a = 5 in.
r_{min} = 0.5555, ok
s/L = 0.0926, ok
a/L = 0.023, ok

Table 4. RBS Example Comparison

W24×76 beam			
	Exact (Chambers and others, 2003)	Exact (this paper)	Regression estimate
Q_{11}	0.896	0.895	0.896
Q_{33}	0.880	0.879	0.881
Q_{55}	0.964	0.964	0.962

The comparison of the three calculated RBS stiffness solutions [this paper (exact), Chambers and others (2003), and regression] is shown in Table 4. The problem conditions are all within the stated bounds of the RBS prequalification and the regression ranges. All the results, in other words from Chambers and others (2003), this paper's exact and estimated values, when put into the Q format for the two flexural and one axial effect, are essentially identical to three significant figures. Even though this is only a single example, it provides solid confirmation of the accuracy of the two independently developed exact solutions here and in Chambers and others (2003), as well as the robustness of the regression estimation alternative.

CONCLUSIONS ON RBS STIFFNESS EFFECTS

One important conclusion from this development is the observation that the resulting range of RBS stiffness reductions of a standard wide flange member relative to its prismatic condition will be the following for the typical space of its design variables:

$$0.8465 \le Q_{11} \le 0.9695$$

$$0.8250 \le Q_{33} \le 0.9662$$

$$0.9250 \le Q_{55} \le 0.9890$$

As expected, the axial reduced stiffness Q_{55} is much less affected than the bending factors Q_{11} and Q_{33}. The dependent Q_{12} reduction can be calculated from Q_{11} and Q_{33}, as given previously, and it will always be slightly lower than Q_{11} for the RBS, up to as much as 8 percent. While many of the potential RBS conditions in its typical design space would indeed experience a flexural stiffness loss of no more than 10 percent, there are more extreme instances wherein this loss could approach 20 percent.

The stiffness reduction regression estimates, and its coefficients, likewise demonstrate the dominant negative effect of the RBS length, *s/L*, and the beneficial contribution of maximizing r_{min}, or equivalently, minimizing the circular cut depth, which is consistent with engineering intuition. As expected, the largest stiffness reductions (almost 18 percent for Q_{33}) occur for the higher *s/L*, in combination with the smaller r_{min} and larger I_f/I input values. Even though *a/L* is positively correlated to Q, *a/L* is a relatively small value and the overall RBS detailing considerations relative to moment gradient effects would usually tend to minimize this distance (place RBS closer to member end) as a trade-off to the necessity for a larger cut, or smaller r_{min}. Consequently, the converse is the best general way to minimize stiffness loss in an RBS: maximize r_{min} and minimize *s/L*, to the extent possible, for the particular beam design conditions.

One obvious way to use the information in this paper is to rigorously follow the steps of this solution and exactly determine the Q_{11}, Q_{12}, Q_{33}, and Q_{55} coefficients, which are all different, followed by their substitution, as illustrated before, in the appropriate terms of the RBS member stiffness matrix outlined in Equation 11. This will result in the

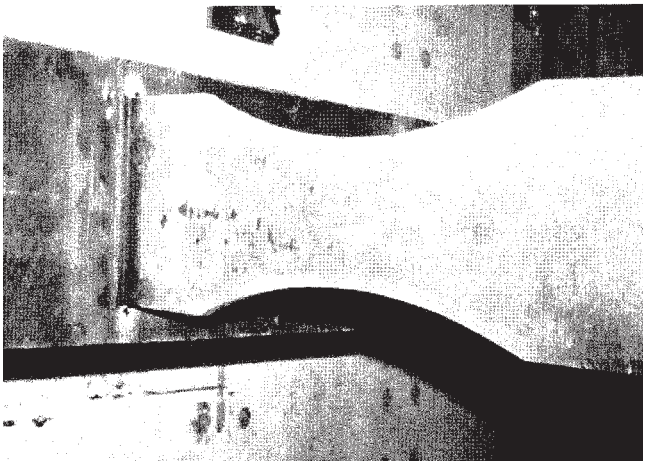

Fig.4. RBS with Circular Cut.

most theoretically accurate nonprismatic stiffness representation.

A quicker alternate approach, but with some approximation, is to realize that Q_{33} is the most often repeating flexural factor in the RBS stiffness matrix, and, hence, also substitute this Q_{33} value for the other two remaining flexural stiffness reductions Q_{11} and Q_{12}. This substitution minimizes calculations to effectively result in a uniform reduction of every flexural stiffness term by Q_{33}. This then leads to the easy design input change from the RBS member original moment of inertia, I, to be replaced by $Q_{33}I$, its effective reduced moment of inertia. Because of the general similarity of Q_{11}, Q_{12}, and Q_{33}, even though rigorously they are numerically different, such a simplification is not expected to introduce large errors.

The axial effect, Q_{55}, can be similarly handled without any loss of accuracy through substituting $Q_{55}A$ as an effective area in place of the full section area, A.

Thus, by simply using "effective" section properties of Q33I and Q55A for an RBS, its stiffness effect can be relatively accurately captured for any type of elastic analysis. This is expected to be an easy and convenient RBS modification of data input to commercial structural software.

Another further simplification and design approximation could be made through use of the estimated linear regression formulas for the reduced stiffness factors instead of their exact solutions, with negligible loss of accuracy, as demonstrated.

One of the RBS design recommendations in Section 3.5.5 of FEMA 350 (FEMA, 2000), states:
"In lieu of specific calculations, a drift increase of 9 percent may be applied for flange reductions to 50 percent of the beam flange width, with linear interpolation for lesser values of beam flange reduction."

As expected, the more exact stiffness solutions presented in this paper indicate that this design approximation may be unconservative in some cases, and over conservative in others, by as much as a factor of 2. Hence, there are clear benefits to checking and using the more exact RBS stiffness properties for some design conditions.

As use of the circular RBS detail shown in Figure 4 continues to grow for high seismicity applications in steel moment frames, this more precise information on its stiffness characteristics, combined with other similar methods for steel design, should enable even faster and better designs, at least in so far as serviceability checking for elastic frame drift and floor deflections.

ACKNOWLEDGMENT

This study was completed as part of the graduate research and thesis of Nestor Iwankiw (Iwankiw, 2002) at the Illinois Institute of Technology under the direction of faculty advisor Jamshid Mohammadi.

The assistance of AISC in encouraging and cosponsoring this independent academic work over the last several years is greatly appreciated. Also, grateful acknowledgment is extended to Arbed, whose original royalty release waiver to their patent provided in 1994 first placed this innovative concept into the U.S. public domain, and enabled the subsequent RBS successes. Many other individuals and organizations, such as those listed in the references, have conducted additional research that substantially contributed to the more complete technical development and widespread acceptance of the RBS for seismic design. Finally, the immense impact on steel seismic design and on the principal author's interests in this field is attributed to the memory of the late Professor Egor P. Popov.

REFERENCES

American Institute of Steel Construction (2002), *Seismic Provisions for Structural Steel Buildings,* ANSI/AISC 341-02, Chicago, IL.

Engelhardt, M.D., Winneberger, T., Zekany, A.J., and Potyraj, T.J. (1996), "The DogBone: Part II," *Modern Steel Construction*, AISC, August, pp. 46-55, Chicago, IL.

Engelhardt, M.D., Winneberger, T., Zekany, A.J., and Potyraj, T.J (1998), "Experimental Investigation of Dogbone Moment Connections," *Engineering Journal*, AISC, Fourth Quarter, pp. 128-139, Chicago, IL

Engelhardt, M.D. (1999), "Design of Reduced Beam Section Moment Connections," *NASCC Proceedings*, AISC, pp. 1-3 to 1-29, Chicago, IL

Chambers, J.J., Almudhafar, S., and Stenger, F. (2003), "Effect of Reduced Beam Section Frame Elements on Stiffness of Moment Frames," J*ournal of Structural Engineering*, ASCE, Vol. 129, No. 3, March, pp. 383-393.

FEMA (2000), *Recommended Seismic Design Criteria for New Steel Moment-Frame Buildings*, FEMA 350, June, Washington, D.C.

Gross, J.G., Engelhardt, M.D., Uang, C.M., Kasai, K., and Iwankiw, N.R. (1999), *Modification of Existing Welded Steel Moment Frame Connections for Seismic Resistance, Design Guide 12*, AISC and NIST, Chicago, IL.

Iwankiw, N.R and Carter, C.J. (1996), "The Dogbone: A New Idea to Chew On," *Modern Steel Construction*, AISC, April, pp. 18-23, Chicago, IL.

Iwankiw, N.R. (1997), "Ultimate Strength Considerations for Seismic Design of the Reduced Beam Section (Internal Plastic Hinge)," *Engineering Journal*, AISC, First Quarter, pp. 3-16, Chicago, IL.

Iwankiw, N.R. (2002), "The Reduced Beam Section Detail–One Method To Improve Seismic Ductility Of Steel Moment Frames," Thesis submitted in partial ful-

fillment of the requirements for the degree of Doctor of Philosophy in Civil Engineering, Illinois Institute of Technology, December, Chicago, IL.

Zekioglu, A., Mozaffarian, M., Le Chang, K., and Uang, C.M. (1997), "Designing After Northridge," *Modern Steel Construction*, AISC, pp. 36-42, March, Chicago, IL.

APPENDIX A

RBS Bending Stiffness Solution

This RBS problem can be non-dimensionalized in terms of *a/L, s/L, I_f /I*, etc. with the primary variable being the *x/L* local coordinates within the RBS length. This conversion allows the RBS rotational stiffness solutions to be obtained in general terms, in other words, *EI/L*, which can then be converted into the desired *Q*, reduced stiffness factors.

The resulting general expressions for the integration over the RBS length "*s/L*" of the conjugate beam loads (areas of real beam bending moment diagram) in terms of the localized abscissa variable *x/L* are:

Left side RBS

$$\frac{K_{11}}{EI_x}=\frac{K_{11}L}{EI}\int_{o}^{\frac{s}{L}}\frac{\left(1-\left(\frac{a}{L}\right)-\left(\frac{x}{L}\right)\right)\left(\frac{dx}{L}\right)}{\left[1-\left(\frac{I_f}{I}\right)\left(1-r_x\right)\right]};$$

Right side RBS (A1)

$$\frac{K_{11}L}{EI}\int_{o}^{\frac{s}{L}}\frac{\left(\frac{a}{L}+\frac{s}{L}-\frac{x}{L}\right)\left(\frac{dx}{L}\right)}{\left[1-\frac{I_f}{I}\left(1-r_x\right)\right]}$$

$$\frac{K_{12}}{EI_x}=\frac{K_{12}L}{EI}\int_{o}^{\frac{s}{L}}\frac{\left(\frac{a}{L}+\frac{x}{L}\right)\left(\frac{dx}{L}\right)}{\left[1-\left(\frac{I_f}{I}\right)\left(1-r_x\right)\right]};$$

(A2)

$$\frac{K_{12}L}{EI}\int_{o}^{\frac{s}{L}}\frac{\left(1-\left(\frac{a}{L}+\frac{s}{L}\right)+\frac{x}{L}\right)\left(\frac{dx}{L}\right)}{\left[1-\frac{I_f}{I}\left(1-r_x\right)\right]}$$

$$A^{RBS}=\int_{0}^{\frac{s}{L}}y\left(\frac{dx}{L}\right) \tag{A3a}$$

$$M^{RBS}=L\int_{0}^{\frac{s}{L}}\left(\frac{x}{L}\right)y\left(\frac{dx}{L}\right) \tag{A3b}$$

using the corresponding *y* integrand function from before for the left or right side RBS, and either K_{11} or K_{12}, where

y = corresponding integrand function of $\int_{0}^{\frac{s}{L}}y\left(\frac{dx}{L}\right)$

$$\left[1-\left(\frac{I_f}{I}\right)\left(1-r_x\right)\right]= \tag{A4}$$

$$\left[1-2\left(\frac{I_f}{I}\right)\frac{\left(\sqrt{\left(\frac{R}{L}\right)^2-\left(\frac{x}{L}-\frac{s}{2L}\right)^2}-\sqrt{\left(\frac{R}{L}\right)^2-\frac{1}{4}\left(\frac{s}{L}\right)^2}\right)}{\left(\frac{b_f}{L}\right)}\right]$$

These RBS equations are related to either the left or right half of the beam, and to either K_{11} or K_{12}, thus, there will always be four different functions of interest. Because of the highly nonlinear nature of these resulting integrands, it was decided to employ numerical integration to compute these K_{11}/EI_x and K_{12}/EI_x areas and their first moments within each "*s/L*" by Simpson's rule. This well documented numerical integration procedure subdivides the total integration space into an even number of discrete "*n*" equal parts, and thereby (*n*+1) value points of the integrand function. Symbolically, Simpson's rule for general integration, based on a quadratic approximation over each integration step, is: $(s/3nL)(y_1 + 4y_2 + 2y_3 + ... 4y_n + y_{(n+1)})$, where y_1, y_2,....$y_{(n+1)}$ are the function values of the integrand at discrete abscissa points that are incremental multiples of (*s/nL*), in other words, $y_1 = y(0)$, $y_2 = y(s/nL)$, $y_3 = y(2s/nL)$, $y_n = ((n-1)(s)/nL)$ and $y_{(n+1)} = y(s/L)$.

The required computations were subdivided into convenient parts for determining the conjugate beam loading area and its first moments (see Figures A1 and A2), in order to isolate the incremental nonlinear effects of the RBS. In general, the approach was to first compute the total effect

within the RBS itself through numerical integration with Simpson's rule

(A_{11}^{RBS} and A_{12}^{RBS} for area, M_{11}^{RBS} and M_{12}^{RBS} for moment),

and then subtract from it the prismatic linear part. (A_{11} and A_{12} for area, m_{11} and m_{12} for moment, respectively.) In the case of the first moments of this loading area, because the RBS functions were always expressed in a local coordinate system *x/L* relative to the left edge of the particular RBS, it was also necessary to transfer the moment of the net RBS area to the left beam end, (MT_{11} and MT_{12}), for the subsequent solution.

Ten integration intervals (n = 10) were used for the application of Simpson's rule in this regard, even though less, probably only about n = 4, would have been sufficiently accurate in view of the robust quadratic nature of the Simpson Rule approximation. Given that this numerical integration was, and can be conveniently programmed for a computer spreadsheet solution, this selection of the optimal number of integration intervals is not critical to the solution efficiency.

Table A1 and Figures A1 and A2 summarize this bending stiffness solution, with separate expressions for the left and right span sides.

For the final equilibrium solution of the conjugate beam, a summation of moments about the left beam end, cancellation of the common [L^2/EI] factor, and substitution of $K_{12} = qK_{11}$ is performed.

Once the RBS carryover factor, q, is inserted into the above equation, with the result that the K_{11} variable cancels, one can directly solve for the only unknown q as a ratio of the entire left side of the equation over the right side:

$$q = \left(\frac{1}{6} + \text{ net } M_{11}^{RBS}(\text{left}) + \text{net } M_{11}^{RBS}(\text{right})\right) \Big/ \left(\frac{1}{3} + \text{net } M_{12}^{RBS}(\text{left}) + \text{ net } M_{12}^{RBS}(\text{right})\right) \quad \text{(A5)}$$

The force equilibrium condition for the conjugate beam (see Figure 3), gives:

$$\frac{K_{11}L}{EI}\left\{\frac{1}{2} + \text{ net } A_{11}^{RBS}(\text{left}) + \text{net } A_{11}^{RBS}(\text{right})\right\} = 1.0 + \frac{K_{12}L}{EI}\left\{\frac{1}{2} + \text{net } A_{12}^{RBS}(\text{left}) + \text{net } A_{12}^{RBS}(\text{right})\right\} \quad \text{(A6)}$$

Again, substitute qK_{11} for K_{12}, with q known from before, and then determine the RBS K_{11} stiffness:

$$K_{11} = 1 \Big/ \left\{\frac{L}{EI}\left(\frac{1}{2} + \text{net } A_{11}^{RBS}(\text{left}) + \text{net } A_{11}^{RBS}(\text{right}) - q\left[\frac{1}{2} + \text{ net } A_{11}^{RBS}(\text{left}) + \text{ net } A_{11}^{RBS}(\text{right})\right]\right)\right\} \quad \text{(A7)}$$

which results, as dimensionally expected, in a multiple of *EI/L*. Q_{11} is simply this final RBS K_{11} value divided by the prismatic rotational stiffness of 4*EI/L*. K_{33}, or Q_{33}, can then be simply calculated as previously indicated in Equations 8 and 6, knowing K_{11} from Equation A7 and q from A5.

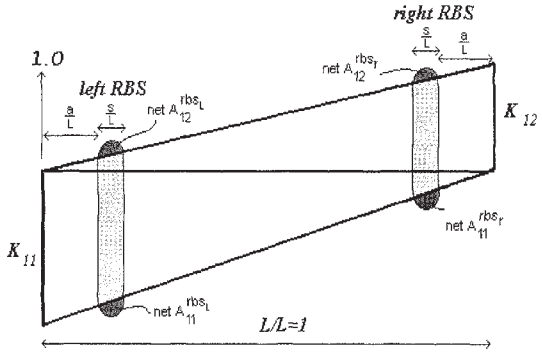

Fig. A1. Conjugate Beam Solution: Overall Geometry and Variables.

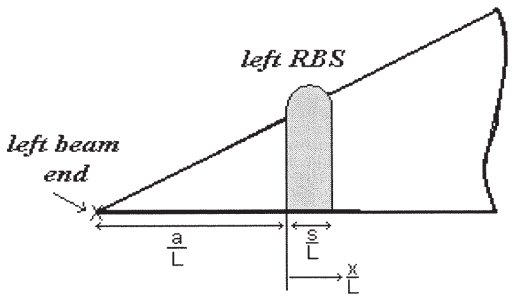

Fig. A2. Conjugate Beam Local Geometry.

Table A1. RBS Bending Stiffness Solution Summary

Methodology:

- Use Simpson's rule for numerical integration of real bending moments, K_{11}/EI_x and K_{12}/EI_x, within each RBS using 10 segments $\left(\frac{dx}{L} = 0.1\left(\frac{s}{L}\right),\ n = 10\right)$
- Integrand functions always referred to left edge of each RBS as zero point of local coordinate system "*x/L*."
- Simpson's rule for area: $0.1L\left(\frac{s}{L}\right)\left(\frac{1}{3}\right)\left\{(y_1)+(4y_2)+(2y_3)....+y_{11}\right\}$
- Simpson's rule for moment: $0.1L\left(\frac{s}{L}\right)\left(\frac{1}{3}\right)\left\{0\,(y_1)+(0.1)\left(\frac{s}{L}\right)(4y_2)+(0.2)\left(\frac{s}{L}\right)(2y_3)....+\left(\frac{s}{L}\right)y_{11}\right\}$

Left RBS	Right RBS
A_{11}^{RBS} = Simpson's rule for area: appropriate y_i	Simpson's rule for area: appropriate y_i
A_{12}^{RBS} = Simpson's rule for area: appropriate y_i	Simpson's rule for area: appropriate y_i
$A_{11} = \frac{K_{11}L}{EI}\left\{1-\left(\frac{a}{L}\right)-\left(\frac{s}{2L}\right)\right\}\left(\frac{s}{L}\right)$	$\frac{K_{11}L}{EI}\left(\frac{a}{L}+\frac{s}{L}-\frac{s}{2L}\right)\left(\frac{s}{L}\right)$
$A_{12} = \frac{K_{12}L}{EI}\left(\frac{a}{L}+\frac{s}{2L}\right)\left(\frac{s}{L}\right)$	$\frac{K_{12}L}{EI}\left(1-\left(\frac{a}{L}+\frac{s}{L}\right)+\frac{s}{2L}\right)\left(\frac{s}{L}\right)$
net $A_{11}^{RBS} = (A_{11}^{RBS} - A_{11})/(\frac{K_{11}L}{EI})$	$(A_{11}^{RBS} - A_{11})/(\frac{K_{11}L}{EI})$
net $A_{12}^{RBS} = (A_{12}^{RBS} - A_{12})/(\frac{K_{12}L}{EI})$	$(A_{12}^{RBS} - A_{12})/(\frac{K_{12}L}{EI})$
M_{11}^{RBS} = Simpson's rule for moment: appropriate y_i	Simpson's rule for moment: appropriate y_i
M_{12}^{RBS} = Simpson's rule for moment: appropriate y_i	Simpson's rule for moment: appropriate y_i
$m_{11} = \frac{K_{11}L^2}{EI}\left[\frac{1}{2}\left(1-\frac{a}{L}\right)\left(\frac{s}{L}\right)^2-\frac{1}{3}\left(\frac{s}{L}\right)^3\right]$	$\frac{K_{11}L^2}{EI}\left[\frac{1}{2}\left(\frac{a}{L}+\frac{s}{L}\right)\left(\frac{s}{L}\right)^2-\frac{1}{3}\left(\frac{s}{L}\right)^3\right]$
$m_{12} = \frac{K_{12}L^2}{EI}\left[\frac{1}{2}\left(\frac{a}{L}\right)\left(\frac{s}{L}\right)^2+\frac{1}{3}\left(\frac{s}{L}\right)^3\right]$	$\frac{K_{12}L^2}{EI}\left[\frac{1}{2}\left\{1-\left(\frac{a}{L}+\frac{s}{L}\right)\right\}\left(\frac{s}{L}\right)^2+\frac{1}{3}\left(\frac{s}{L}\right)^3\right]$
$MT_{11} = \left(\frac{K_{11}L^2}{EI}\right)\left(\text{net } A_{11}^{RBS}\right)\left(\frac{a}{L}\right)$	$\left(\frac{K_{11}L^2}{EI}\right)\left(\text{net } A_{11}^{RBS}\right)\left[1-\left(\frac{a}{L}+\frac{s}{L}\right)\right]$
$MT_{12} = \left(\frac{K_{12}L^2}{EI}\right)\left(\text{net } A_{12}^{RBS}\right)\left(\frac{a}{L}\right)$	$\left(\frac{K_{12}L^2}{EI}\right)\left(\text{net } A_{12}^{RBS}\right)\left[1-\left(\frac{a}{L}+\frac{s}{L}\right)\right]$
net $M_{11}^{RBS} = (M_{11}^{RBS} - m_{11} + MT_{11})/(\frac{K_{11}L^2}{EI})$	$(M_{11}^{RBS} - m_{11} + MT_{11})/(\frac{K_{11}L^2}{EI})$
net $M_{12}^{RBS} = (M_{12}^{RBS} - m_{12} + MT_{12})/(\frac{K_{12}L^2}{EI})$	$(M_{12}^{RBS} - m_{12} + MT_{12})/(\frac{K_{12}L^2}{EI})$